On Single Station Forecasting: The Geopotential Height, its Vertical and Times Structure and 500 mbar ARMA Prediction

Klaus Fraedrich and Thomas Dümmel

Institut für Meteorologie, Freie Universität Berlin, D-1000 Berlin 33, W-Germany

(Manuscript received 23.08.1982, in revised form 03.01.1983)

Abstract:

Two eigenvectors are necessary to explain about 99 % of the vertical and time variability of tropospheric geopotential height observations at a single station (Berlin). Their structures and amplitudes characterize an equivalent barotropic (external) and baroclinic (internal) mode of purely tropospheric dynamics which are associated with two distinct time scales of about 5–6 and 2–3 days. An univariate stochastic ARMA process is selected and applied to the amplitude of the barotropic eigenvector for predicting the 500 mbar geopotential height and its probability distribution up to a lead time of several days ahead. The model is verified by hindcasting the observations used for model fitting and by independent predictions. In combination with climatology and persistence, the forecast by ARMA processes provides another stringent evaluation standard of comparison for numerical weather prediction models, which allows a phase prediction of highs and lows. The advantage is a forecast skill which is generally better than persistence and climatology.

Zusammenfassung: Zur Stationsvorhersage (2. Teil): die vertikale und zeitliche Struktur des Geopotentials und 500 mbar ARMA-Vorhersage

Zwei Eigenvektoren sind notwendig, um etwa 99 % der vertikalen und zeitlichen Variabilität des troposphärischen Geopotentials an einer Station (Berlin) zu beschreiben. Die vertikalen Profile und das zeitliche Verhalten der Amplituden der Eigenvektoren charakterisieren die äquivalent-barotropen (externen) und baroklinen (internen) Verhältnisse der ausschließlich troposphärischen Dynamik. Zu diesen externen und internen Moden gehören zwei unterschiedliche Zeitmaßstäbe von 5–6 und 2–3 Tagen. Ein Univariater, stochastischer ARMA-Prozeß wird auf die Vorhersage der Amplitude des barotropen Eigenvektors angewandt, um die geopotentielle Höhe des 500 mbar Niveaus für mehrere Tage vorherzusagen. Das Modell wird durch die Beobachtungen verifiziert, an denen es geeicht worden ist sowie durch unabhängige Vorhersagen. Zusätzlich zur Klimamittel- und Persistenz-Prognose ist der ARMA-Prozeß ein weiteres Standard-Modell, mit dem die Güte numerischer Wettervorhersage-Modelle lokal verglichen werden kann, zumal Vorhersagen der Phasen von Hochs und Tiefs damit möglich sind.

Résumé: Sur la prévision à une seule station (2e partie): la structure verticale et temporelle du géopotentiel et la prévision ARMA à 500 mbar.

Deux vecteurs propres sont nécessaires pour expliquer environ 99 % de la variabilité verticale et temporelle de l'altitude géopotentielle troposphérique à une seule station (Berlin). Les profils verticaux et le comportement temporel des amplitudes des vecteurs propres caractérisent les modes barotrope équivalent (externe) et barocline (interne) de la dynamique purement troposphérique. A ces modes sont associées deux échelles de temps distinctes de 5–6 et 2–3 jours. Un processus stochastique univarié ARMA est appliqué à l'amplitude du vecteur propre barotrope pour prédire l'altitude géopotentielle à 500 mbar et sa distribution en probabilité à plusieurs jours d'échéance. Le modèle est vérifié à l'aide des observations utilisées pour l'ajustement du modèle et à l'aide de prévisions indépendantes. Combinée avec la climatologie et la persistance, la prévision par le procédé ARMA fournit une autre évaluation standard pour comparer la qualité de modèles numériques de prévision du temps, permettant la prévision des dépressions et des zones de haute pression.

0005-8173/83/02 0221-19 $ 02.00/0

1 Introduction

Weather forecasting is generally based on a network of many stations with various weather elements; numerical and statistical weather predictions apply physical theory and empirical procedures, respectively, to make these forecast objective. Compared with such a comprehensive background of data and theory, forecasts using only single station observations appear inferior. But local weather data can instantaneously be incorporated into suitable prediction models to guide a single station forecaster (see for example FRAEDRICH and MÜLLER, 1983). Although local rawinsonde ascents contain much information, particularly if time series are considered, this information has been used mainly to describe atmospheric processes. Therefore an extension of these investigations towards a single station forecasting is the subject of this paper applying autoregressive moving average (ARMA) models. They are particularly useful in forecasting naturally persistent time series as occurring in geophysics (see e.g. KATZ and SKAGGS, 1981). Before model building it appears necessary to reduce the data set to its basic meteorological content suitable for prediction. Thus, the analysis will be confined to daily geopotential height profiles on selected pressure levels. In Section 2 the vertical structure of the atmosphere is characterized by empirical orthogonal functions (EOF) of the geopotential height below the tropopause representing only tropospheric dynamics. The behaviour in the time domain is described by the related amplitudes of the vertical EOF's and their spectra (Section 3). Finally, a purely stochastic ARMA model is deduced (Section 4) to forecast the 500 mbar geopotential at a single station. Besides climatology and persistence forecasts it should be applicable as a regionally relevant evaluation standard for numerical weather predictions.

2 The vertical structure of the troposphere

The data set analysed consists of daily radiosonde observations of the geopotential height Z (gpm) on nine selected pressure levels from 950 to 300 mbar at Berlin-Tempelhof (52°29'N, 13°25'E and 46 m elevation). The standard sample runs ten years from 1970 through 1979. Seasonal sets of 120 days are extracted for the analysis; the ten summer seasons start on 1 May, the ten winter seasons on 1 November. Additionally, the summer 1980 and winter 1980/81 seasons are used as a separate and independent data set.

Data analysis: The observed geopotential height $Z(p, t)$ is a time-dependent variable on discrete pressure levels p and is represented by empirical orthogonal functions:

$$Z(p, t) = \langle Z(p, t) \rangle + \sum_{n=1}^{N} c_n(t)\, Z_n(p) + \mathrm{res}(p, t) \tag{2.1}$$

where $\langle\,\rangle$ is the seasonal or ensemble average in time, $c_n(t)$ the time-dependent amplitude or coefficient, $Z_n(p)$ the space function (EOF or eigenvector) with its components on the discrete pressure levels p, N is the truncation limit of the EOF expansion, res (p, t) the residuum of the series expansion. The space functions of EOF's $Z_n(p)$ are determined from the observed sample $Z(p, t)$ by standard methods. They are orthogonal and normalized to their corresponding eigenvalues λ_n^2:

$$\sum_{p} Z_n(p)\, Z_m(p) = \delta_{n,m}\, \lambda_n^2 \tag{2.2}$$

where $\delta_{n,m}$ is the Kronecker delta ($\delta_{n,m} = 0; 1$ for $n \neq m; n = m$). Thus, the units related to an eigenvector $Z_n(p)$ or its components are the same as the units of the data set $Z(p, t)$; their magnitudes, however, provide a direct measure of the time variability (in terms of the standard deviation) of the data as it can be explained by the eigenvector components.

The time-dependent coefficients $c_n(t)$ related to each EOF $Z_n(p)$ are orthogonal and normalized to one: $< c_n c_m > = \delta_{n,m}$. Thus, the vertical variance of an individual profile of the geopotential height deviation explained by N EOF's is

$$\sigma^2(t) = \sum_{n=1}^{N} c_n^2(t)\,\lambda_n^2 \quad (\text{in gpm}^2) \tag{2.3}$$

which leads to the total variance of the vertical and time sample

$$<\sigma^2(t)> = \sum_{n=1}^{N} <c_n^2(t)>\lambda_n^2 = \sum_{n=1}^{N} \lambda_n^2 \quad (\text{in gpm}^2) \tag{2.4}$$

i.e., the total variance explained by $Z_n(p)$ and its coefficient $c_n(t)$ is simply given by the corresponding eigenvalue λ_n^2 with $< c_n^2(t) > = 1, < c_n > = 0$.

Pressure intervals or weighting functions $dp/\Delta p$ may be attached to each component of an eigenvector. They are normalized by $\sum_p dp/\Delta p = 1$, where $\Delta p = \sum_p dp$ is the total pressure interval, dp is the pressure interval related to each pressure level p. These weighting functions have no influence on the structure of the space functions $Z_n(p)$ but on their magnitudes; comparison with HOLMSTRÖM's (1963) eigenvectors is now possible after multiplication of $Z_n(p)$ by $\sqrt{\Delta p/dp}$ at each level. The analysis of the data set leads to space functions $Z_n(p)$ after eliminating the seasonal mean vertical profile $< Z >$ for both all summer and all winter seasons combined.

General structure: Only two eigenvectors are needed to explain more than 99 % of the total space-time variance of the seasonal data samples. These eigenvectors are shown in Figure 1. The first eigenvector $Z_1(p)$ covers about 91–93 % of the total variance (summer: 91.2 %, winter: 92.6 %). It can be related to the dominating barotropic or divergent barotropic mode of tropospheric dynamics and is comparable with the external mode deduced by normal mode analysis (e.g. KASAHARA, 1976; GAVRILIN, 1965). The second eigenvector $Z_2(p)$ explains almost all of the remaining variance (summer: 8.2%, winter: 7.0%). It can be related to the baroclinic nature of tropospheric dynamics and to the first internal mode in connexion with normal mode analysis. From the observational point of view the relationship between the space functions $Z_1(p)$, $Z_2(p)$ and the tropospheric dynamics will be discussed in terms of the spectra of their time-dependent amplitudes or coefficients $c_{1,2}(t)$ (Section 3).

Seasonal variability: The basic structure of the first and second eigenvector evolves after a sequence of 10 to 20 days of local soundings. This is about the largest period resolvable from the variance produced by tropospheric dynamics, where periods ranging from cyclones (< 5 days) and cyclone families (5–12 days) to high-low-index vacillations (> 12 days) are included. Furthermore, the vertical profiles and the magnitudes of the eigenvector components hardly vary from season to season indicating their stability. Observed extrema of an upper and lower level EOF-component are: Z_1 (300 mbar) $\sim -0.49, -0.59$; Z_2 (300 mbar) $\sim -0.39, -0.52$; Z_1 (950 mbar) $\sim -0.14, -0.23$; Z_2 (950 mbar) $\sim 0.40, 0.45$, where the summer–winter difference is included. These numbers (normalized by the seasonal standard deviations λ_n) are taken from first and second eigenvectors and eigenvalues λ_n^2, which are separately determined for each individual season with its own seasonal average profile eliminated. As expected, however, the total variances (or eigenvalues λ_n^2) of individual seasons vary considerably, but leaving the structure of the space functions $Z_n(p)$ almost unchanged (summer: $\lambda_1^2 \sim 40$–77, $\lambda_2^2 \sim 3$–7.5; winter: $\lambda_1^2 \sim 90$–200, $\lambda_2^2 \sim 9$–13 in 10^3 gpm^2).

Stratospheric levels: If four lower stratospheric levels (250, 200, 150, 100 mbar) are added to the EOF analysis, the structure of the eigenvectors changes considerably. Three eigenvectors are necessary to explain about 99 % of the observed total variance. This is illustrated by the three EOF's deduced from

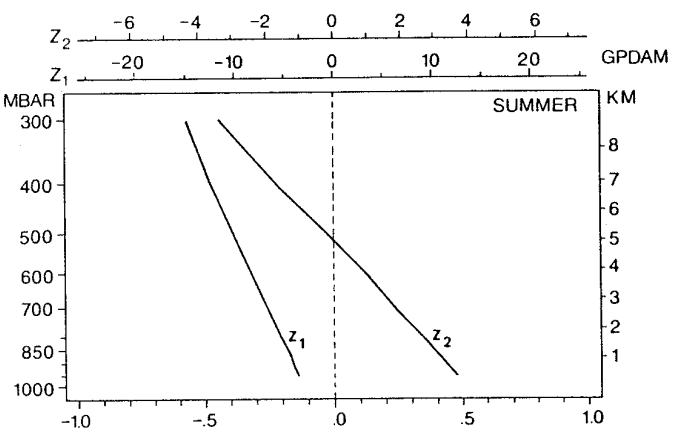

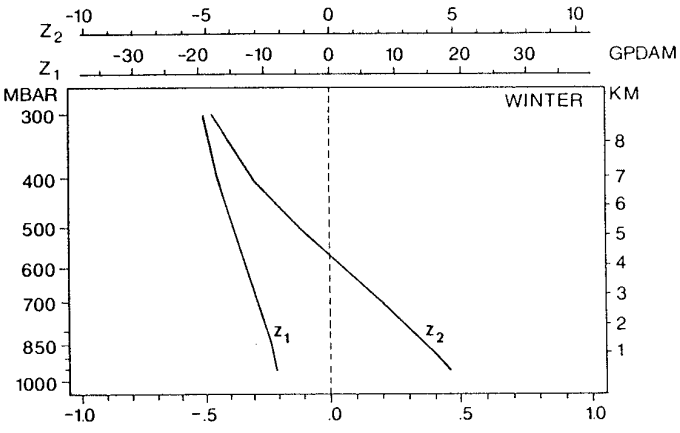

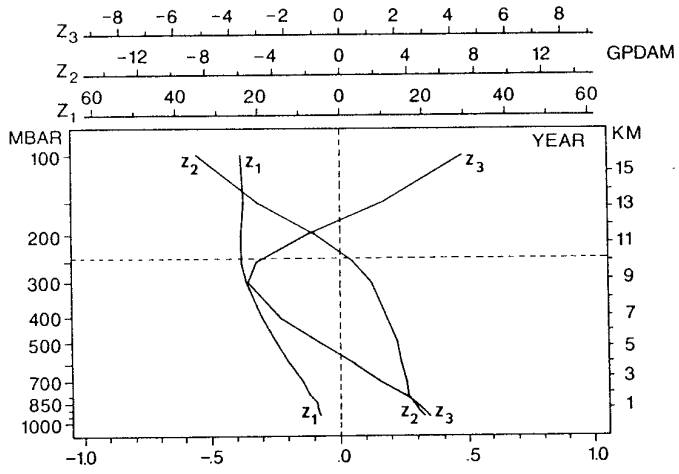

● **Figure 1a–c**

Empirical orthogonal functions (EOF's or eigenvectors) of the vertical structure of the geopotential height at a single station (Berlin); two tropospheric eigenvectors Z_1 and Z_2 for summer (a) and winter (b), and three annual tropospheric plus stratospheric eigenvectors (c) describe 99 % of the seasonal or annual space-time variance. The units of the top abscissa are defined by the related eigenvalues in terms of a standard deviation (gpm), the bottom abscissa is dimensionless.

● **Bild 1a–c**

Empirische orthogonal-Funktionen (EOF's oder Eigenvektoren) der Vertikalstruktur der geopotentiellen Höhe an einer Station (Berlin); zwei troposphärische Eigenvektoren Z_1 und Z_2 für Sommer (a) und Winter (b) sowie drei Eigenvektoren für Troposphäre und Stratosphäre beschreiben 99 % der jahreszeitlichen bzw. jährlichen vertikalen zeitlichen Varianz. Die oberen Abscissen sind in Einheiten der Standardabweichung definiert; die unteren sind dimensionslos.

the complete ten year data set (Figure 1c) with seasonal variations included. Their eigenvalues λ_1^2 = 40.0, λ_2^2 = 2.4, λ_3^2 = 0.8 (in 10^4 gpm^2) describe 92.2, 5.5 and 2.0% of the total space-time variance (summer: 89.6, 5.8, 3.0%, winter: 90.6, 5.8, 3.0%).

The structures of these three eigenvectors (Figure 1c) below tropopause can be compared with the two eigenvectors deduced from purely tropospheric data (Figures 1a, b). The first EOF's (Z_1) of each set are similar as well as the third EOF Z_3 (of the stratosphere plus troposphere sample) compared with the second ones (Z_2) of the purely tropospheric data set. However, another EOF (of rank two) occurs, if the stratospheric levels are included. This EOF Z_2 (Figure 1c) describes the second largest amount of variance (i.e., it is related to the second eigenvalue). As the vertical profile changes its sign at the tropopause, it characterizes the lower stratosphere compensating the tropospheric processes which, of course, include baroclinic effects in the troposphere. The related amplitude spectra support this conclusion. Their variance densities are distributed amongst short, long and ultra-long period disturbances. There is almost no time-scale preference, which, however, is observed for the external and first internal mode of the purely tropospheric eigenvectors.

Highs and lows: Four different types of tropospheric weather systems can be distinguished by upper and lower level geopotential height deviations from a synoptic scale area average: cold and warm lows, cold and warm highs. At a single station this is possible only, if the seasonal time average $<Z(t, p)>$ of the geopotential height can be exchanged by a suitable and synoptically representative area average $[Z(p, t)]$ for any time of observation, i.e. $<Z(t, p)> = [Z(p, t)]$. This is assumed in the following.

Based on the truncated EOF-expansion (2.1) the local height deviations $\Delta Z(p, t)$ in time are defined with high accuracy by two eigenvectors $Z_{1,2}$ and their time-dependent amplitudes $c_{1,2}$:

$$\Delta Z(p, t) = Z(p, t) - <Z(t, p)> = \sum_{n=1}^{2} c_n(t) Z_n(p) \tag{2.5}$$

Replacing the synoptic scale area average $[Z(p, t)]$ by the seasonal long time mean $<Z(p)>$ one obtains a cold low (warm high), if $\Delta Z < 0$ (> 0) at p = 950 and 300 mbar; whereas warm lows (cold highs) are defined by $\Delta Z < 0$ (> 0) at p = 950 mbar and $\Delta Z > 0$ (< 0) at p = 300 mbar. The definition of lows or highs refers to the lower pressure level. These four systems are separable from one another by the two conditions: $\Delta Z(p, t) = 0$ at p = 950, 300 mbar (2.5).

But, instead of the two conditions of vanishing upper and lower level height deviations, $\Delta Z(p, t) = 0$, the two EOF-amplitudes $c_1(t)$, $c_2(t)$ can be used to separate the four systems, given the eigenvectors $Z_1(p)$ and $Z_2(p)$, or their components, respectively, at p = 950 and 300 mbar:

$$c_1 Z_1(p) + c_2 Z_2(p) = 0 \tag{2.6}$$

This leads to two "separatices" dividing highs from lows and warm cores from cold cores.

The results are shown schematically in the (c_1, c_2)-space (Figure 2). Further information on the upper level structure may be gained: Warm lows are defined by a surface low with a warm core in the mid-troposphere. Whether there is an upper layer high or low pressure system (extending from the mid-troposphere upwards) sufficient to keep the core warm depends on the surface amplitude. Thus, the level of change from upper low to high can be determined by additional separating lines in the (c_1, c_2)-space improving the schematic diagram. The opposite holds for cold highs.

The coefficient c_1 associated with the first eigenvector predominatly describes changes from cold lows to warm highs (and vice versa) and intermediate stages of their development or local realization. These are systems modifying the upper and lower troposphere in the same sense, i.e. they are mainly barotropic. The coefficient c_2 associated with the second eigenvector indicates the change from warm low to cold high (and vice versa) modifying upper and lower troposphere in an opposite sense, i.e.

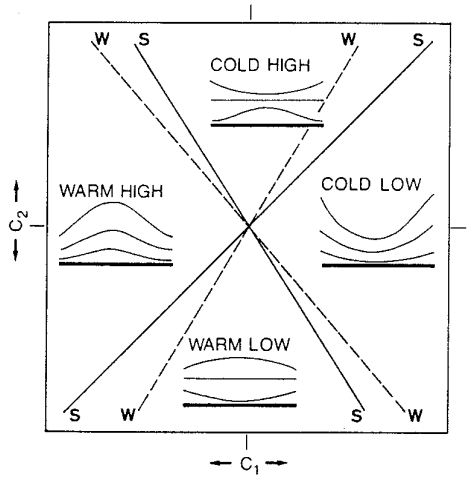

- **Figure 2**
  Schematic thermal structure of synoptic disturbances classified by the coefficients c_1 and c_2 of the two geopotential height eigenvectors Z_1 and Z_2 in winter (W) and summer (S).

- **Bild 2**
  Klassifikation der thermischen Struktur synoptischer Störungen mit Hilfe der Koeffizienten (Amplituden) c_1 und c_2 der beiden Eigenvektoren Z_1 und Z_2 des Geopotentials in Winter (W) und Sommer (S).

these systems are mainly baroclinic. This synoptic and dynamic classification of the EOF-coefficients allows a useful meteorological interpretation of time trajectories in the (c_1, c_2)-space. They characterize sequences of weather systems by single station observations, provided that the assumed space-time average exchange holds, i.e. $[Z(p, t)] = \langle Z(t, p) \rangle$. An illustrative example follows.

The W-European drought (August 76): This event has been discussed from the British Isles' point of view, where it was most severe (e.g. GREEN, 1977). It also affected the eastern parts of W-Europe. From the Berlin point of view the time development of this episode is shown by the time trajectory in the (c_1, c_2)-space starting at 4 August and lasting 24 days until 27 August (Figure 3a). The trajectory of the whole episode starts and ends near the climatic summer average ($c_{1,2} \sim 0$) and describes an almost closed orbit in the warm high basin. A close examination reveals that most of the time the local trajectory moves along and across the separatrix between the cold and warm high sections representing both divergent barotropic and baroclinic dynamics. Upper troughs erode the warm core system and lead to its disappearence at the end of this episode. These two synoptic systems (warm and cold high) have the surface high situation in common but can be distinguished in the upper layer by a ridge (warm high) or a trough (cold high). Thus, the time average over the trajectory in the (c_1, c_2)-space at Berlin yields an intermediate situation between upper trough and ridge but a surface high (anticyclone). The comparison with available monthly averaged maps (Figure 3b, c; 300 and 850 mbar) and, of course, daily ones (which are not shown) supports the results from the purely local interpretation. It should be noted that this summer has not been EOF-analysed individually but as one out of ten, using the ensemble (10 summer seasons) averaged $\langle Z \rangle$ and the related standard EOF's with their coefficients. Other weather sequences can be selected to demonstrate equally good agreement between the space and local time structures. We conclude (until later disproved) that the space-time average exchange does not lead to serious misinterpretation.

3 The structure in the time domain

The coefficients $c_{1,2}(t)$ related to the space functions $Z_{1,2}(p)$ of the purely tropospheric data set are statistically analysed to describe the behaviour in the time domain for winter and summer seasons.

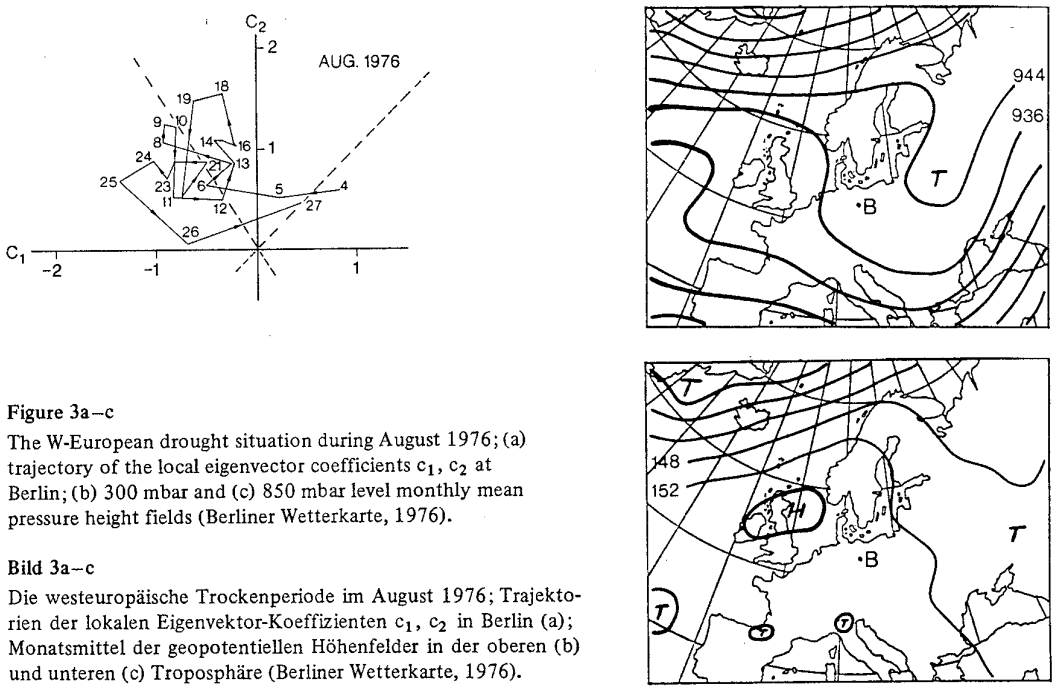

- **Figure 3a–c**
  The W-European drought situation during August 1976; (a) trajectory of the local eigenvector coefficients c_1, c_2 at Berlin; (b) 300 mbar and (c) 850 mbar level monthly mean pressure height fields (Berliner Wetterkarte, 1976).

- **Bild 3a–c**
  Die westeuropäische Trockenperiode im August 1976; Trajektorien der lokalen Eigenvektor-Koeffizienten c_1, c_2 in Berlin (a); Monatsmittel der geopotentiellen Höhenfelder in der oberen (b) und unteren (c) Troposphäre (Berliner Wetterkarte, 1976).

Histogram: The frequencies of the daily coefficients $c_{1,2}$ are almost Gaussian distributed (Figure 4) around the climatological mean ($c_1 = c_2 = 0$). A circle of radius $2 \ln (100/100\text{-}\alpha)^{1/2} \sim 1.5$ centered at $c_1 = c_2 = 0$ contains the standard deviation of a normal distribution ($\alpha = 68.3$). This graphical illustration allows a visual control of the normal distribution of the data before Gaussian processes are applied.

The climatic mean (or local ensemble average) is not really identical with the modal value. The most frequent or long lasting weather systems at Berlin (representative for the continental part of W-Europe) are warm highs with divergent barotropic dynamics. They are dominating the summer seasons more than the winter. Less frequent are cold lows. Particularly during summer they have to be relatively strong in order to balance the more frequent but relatively weak warm high situations, to obtain the climatic mean. Secondary maxima may be identified along the "separatrix" between cold lows and cold highs; i.e. upper level troughs of rather strong baroclinity ($c_2 >> 0$) but hardly affecting the surface pressure field (i.e. cut-off cyclones, etc.). Finally, it should be noted that the synoptic interpretation (besides the dynamic one) is based on the space-time average exchange (Section 2).

Spectral estimation, significance and time scales: The seasonal time series $c_{1,2}(t)$ are transformed to obtain power spectra. Computing the spectra, the lag-correlation method is applied (maximum lag 32 days) to which removal of a linear trend and application of a lag window is implicit (JENKINS and WATTS, 1968). The Tukey window is used with an equivalent band width of 0.04167 cycles per day. An area conserving transformation is applied by which the meteorologically relevant phenomena are emphazised at the higher frequency end of the spectrum: the spectral densities are multiplied by frequency and displayed on a logarithmic frequency scale labelled according to the period in days. The results show computed variance densities averaged for the winter and summer seasons. The ensemble averages are enveloped by the seasonal standard deviation (shaded) and their extrema (dotted) to indicate stability and similarity of the seasonal spectra.

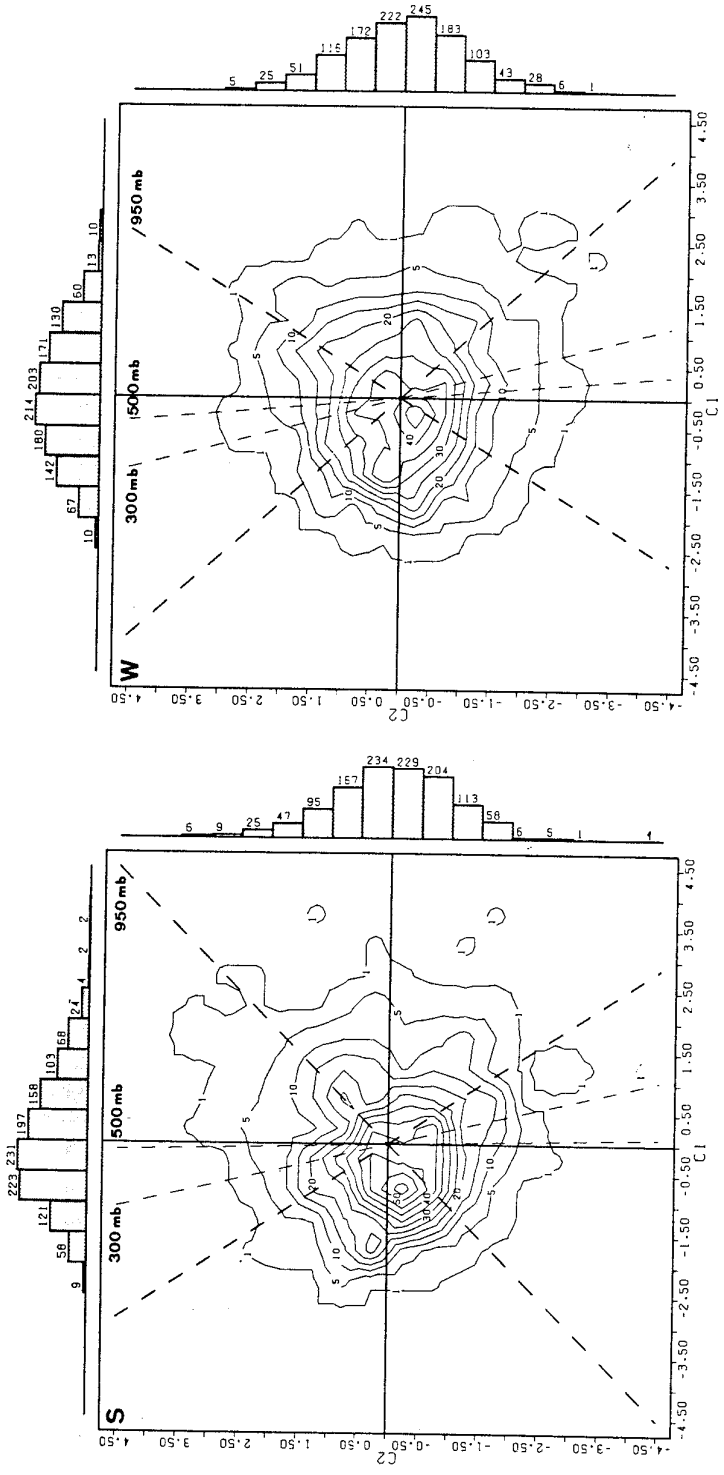

Figure 4 Frequency distribution of eigenvector coefficients for summer and winter. The broken lines separate highs from lows at three topospheric levels (300, 500, 950 mbar) and warm from cold cores (see Figure 2).

Bild 4 Häufigkeitsverteilung der Eigenvektor-Koeffizienten für Sommer und Winter. Die gestrichelten Linien trennen Hochs und Tiefs in den drei Höhen 300, 500 und 950 mbar und kalte von warmen Kernen (siehe Bild 2).

The observed seasonally averaged spectra are tested against the common null hypothesis of a discrete first order autoregressive AR(1) or Markov process c(t) with the time step $\Delta = 1$ day and the related power spectrum p(f):

$$c(t) = \phi_1 c(t-\Delta) + a(t)$$
$$p(f) = 2\Delta s_c^2 (1-\phi_1^2)/(1+\phi_1^2 - 2\phi_1 \cos 2\pi f\Delta) \quad (3.1)$$

The parameters of the process c(t) are deduced from initial estimates, i.e. fitted to the data (without linear trend) by the lag 1 autocorrelation $\phi_1 = <c(t)\, c(t-\Delta)>/<c^2(t)>$ and by the time series variance $s_c^2 = <c^2(t)> = 1$. The AR(1) process is forced by a white noise a(t) of zero mean and a variance $s_a^2 = <a^2(t)> = s_c^2 (1-\phi_1^2)$. The serial correlation coeffient ϕ_1 is related to the relaxation time scale τ of the corresponding continuous Markov process

$$\tau = \frac{\Delta}{1-\phi_1} \quad (3.2)$$

The relaxation time scales $\tau_{1,2}$ are different for both eigenvectors $Z_{1,2}$. The divergent barotropic mode is characterized by the longer time scale τ_1

	τ_1	τ_2	
Su	5.3	3.1	days
Wi	5.4	2.2	days

i.e. the atmosphere's linear memory is longer for slow divergent barotropic changes (Z_1) between warm high-cold low situations than for τ_2 of the purely baroclinic activity (Z_2) of migrating fronts and cyclones. Besides their meteorological interpretation, the time scales $\tau_{1,2}$ allow a more realistic estimate of the degrees of freedom (relevant to any significance test) by reducing the 120 days of observations per season to approximately $120/\tau$ statistically independent realizations.

The choice of the first order Markov-process as null-hypothesis is based on the relatively large relaxation time scales τ indicating a significant linear correlation ($\phi_1 \geqslant 0.5$) between consecutive days for all time series; k further lags still fulfill $\phi_k \sim \phi_1^k$. However, white noise could also be a relevant null-hypothesis particularly for the second (or baroclinic) mode Z_2 due to its shorter period fluctuations. Therefore, the c_2-series are tested against both red and white noise the latter having the same spectral density for all frequencies $2 s_c^2 \Delta$ (i.e. eq. 3.1 for $\phi_1 = 0$.). An a priori significance level of 95% for selected frequency bands is chosen due to prior knowledge of the related meteorological phenomena from different data sets (e.g. BÖTTGER and FRAEDRICH, 1980) and circulation models (e.g. HAYASHI and GOLDER, 1977). Three peaks at short (< 5 days), long (5–12 days) and ultra-long (> 12 days) periods are tested to be distinct from the red and white noise spectra. When ensemble averaged over the ten summer seasons, the ultra-long period of the divergent barotropic mode and the long period disturbances of the baroclinic and barotropic mode contribute variance beyond the 95 % significance level of ensemble averaged red noise. For the winter seasons, only the 8–15 day period disturbances of both the first and second EOF are about to reach this significance level. However, no seasonal ensemble average peak is significant, if the more realistic degrees of freedom (d.o.f) based on independent data (i.e. reduced by the appropriate time scales) are used. The confidence limits are given by the chi-squared distribution; the d.o.f. are estimated by (2N-m/2)/m with the number of days reduced to statistically independent observations $N = (1200 \text{ days})/\tau$, the maximum lag m = 32, and a weighting factor of 4/3 due to application of the Tukey window (JENKINS and WATTS, 1968).

Two conclusions can be drawn from these results:

(i) Any physical interpretation of the peaks (in the following subsection) remains merely qualitative. Additionally, the predominating periods have hardly any predictive value on the regional or local scale.

Nevertheless, the spectral peaks are still meteorologically meaningful, for they occur in almost all individual seasons. However, they vary in intensity and preferred period because single station observations are rather sensitive to small regional displacement of large-scale phenomena.

(ii) A statistical single station forecast seems to provide a reasonable approach because red and white noise processes are able to describe much of the observed spectral variance distribution, at least in an averaged sense. Some methods of univariate stochastic predictions are applied (Section 4) to obtain purely statistical standards of single station forecast skills of geopotential height.

Vacillation, cyclone families and cyclones: Figure 5 shows clearly that the EOF Z_1 describes longer periods: There are variance contributions by ultra-long periods (> 12–15 days), which can be related to the barotropic or external mode Z_1 only. They are synoptically realized by longer lasting warm highs followed (and preceeded) by cold lows (see interpretation of histogram). The relatively shorter periods (< 12 days) are dominated by the first internal or baroclinic mode Z_2 with cyclones (< 5 days) and cyclone families (5–12 days). Here it should be realized that the spectra are normalized by variance, i.e. $\lambda_1^2 >> \lambda_2^2$ (Section 2).

Spectral densities of both the divergent barotropic Z_1 and the baroclinic Z_2 modes occur in the 10–15 day period interval in winter. This indicates the existence of a vacillation or index cycle, which consists of a baroclinically active part with maximum length of about 10–15 days (cyclone families) or shorter (cyclones), plus a more inactive part of about the same length; thus a period of 20–30 days is obtained. The barotropic mode (Z_1) participates in both the quiescent and synoptically more active phase of the cycle when excited by major slowly progressive waves (cold lows). These waves define the lower time scale limit for divergent barotropic mode dynamics with a period of about 10 days. The baroclinic mode (Z_2) has an upper limit at about the 15 day period. Therefore, it can be concluded from this overlapping that the vacillation cycle is effected by both baroclinic and barotropic dynamics (at least during the phase of transition).

4 ARMA prediction of the local 500 mbar geopotential height

As the baroclinic or second eigenvector Z_2 changes sign in the mid-troposphere, it does not contribute to the 500 mbar geopotential height variations which, therefore, are almost completely determined by the 500 mbar component of the first eigenvector Z_1 (500 mbar) multiplied with the time-dependent coefficient $c_1(t)$. However, the accuracy of the first EOF to describe the complete geopotential height structure decreases from almost perfect at 500 mbar towards both higher and lower levels due to the missing baroclinic mode. There are two data sets available to fit univariate stochastic models for predicting the 500 mbar geopotential height. They can physically be interpreted as statistical analogies of (i) "barotropic" forecasting: both predictor and predictand are taken from the same data set, which is the 500 mbar geopotential at a single station, and (ii) "equivalent barotropic" forecasting: the amplitude $c_1(t)$ of the first eigenvector Z_1 serves as predictor, whereas the predictand (i.e. the local 500 mbar height) is approximated by the product of the 500 mbar component of the first EOF Z_1 (500 mbar) and the predicted coefficient c_1. The emphasis of this section lies on "equivalent barotropic" forecasting at a single station.

Forecasts made by univariate statistics, e.g. chance, persistence or climatology, provide the common standards of comparison to evaluate the utility of numerical weather prediction models. In the following a purely stochastic univariate model is developed to serve as an improved evaluation standard of comparison and a guidance for local forecasters. It is applied to the 500 mbar height at a single station.

The ARMA model: Mixed autoregressive (order p) moving average (order q) or ARMA (p, q) models are only a first approximation to simulate meteorological observations c(t) for t = 1,2 ..., because they

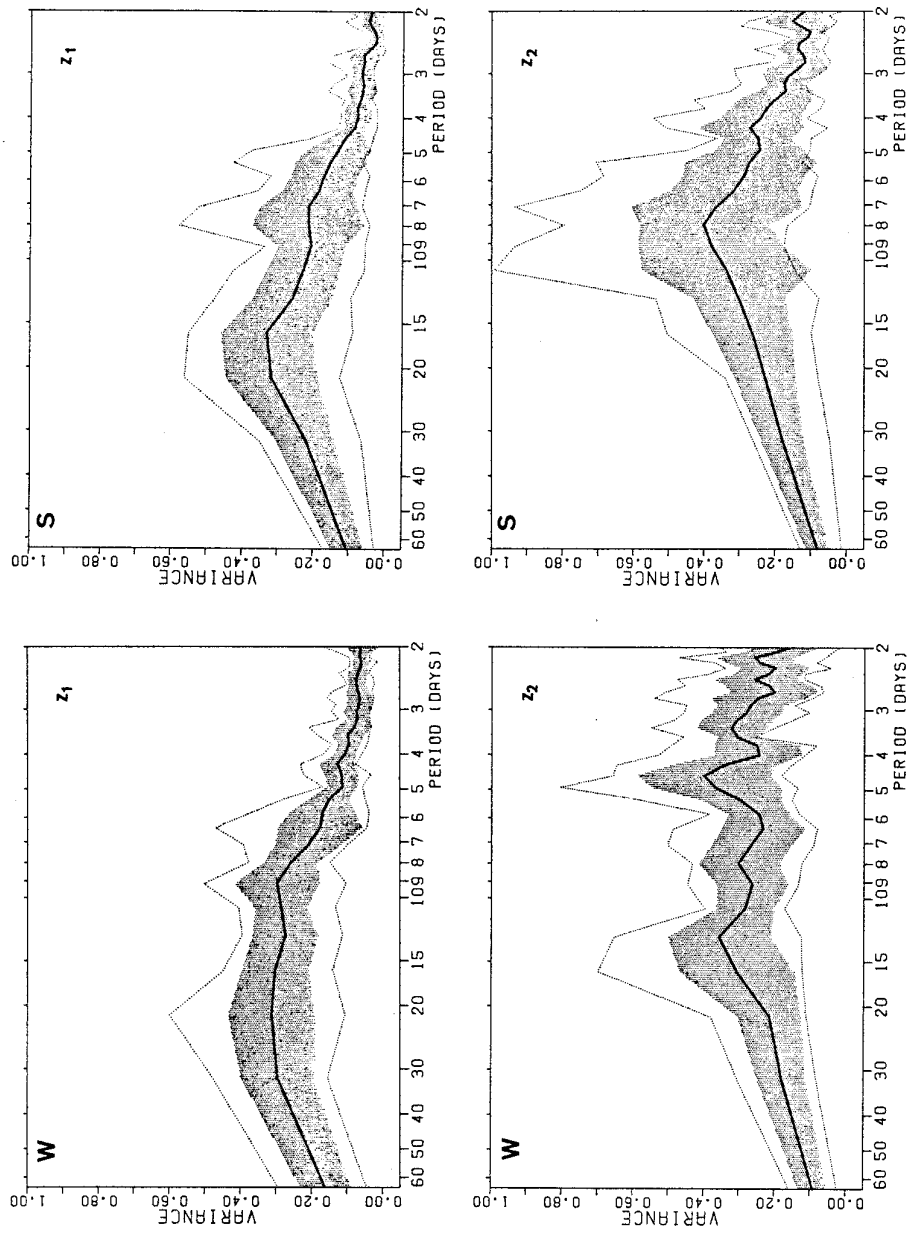

Figure 5 Power spectra of the eigenvector coefficients for summer (S) and winter (W) seasons. The seasonal ensemble average (full line), the related standard deviation (shaded area) and the extrema (dotted line) of individual seasons are frequency-multiplied power spectra in units of variance.

Bild 5 Power-Spektren der Eigenvektor-Koeffizienten für Sommer (S) und Winter (W). Die jahreszeitlichen Ensemble-Mittel (durchgezogen), deren Standardabweichung (schattiert) und Extrema (punktiert) einzelner Saisons sind dargestellt als frequenzgewichtete Power-Spektren in Varianzeinheiten.

define a stationary stochastic process. An ARMA process (as described in textbooks: BOX and JENKINS, 1976; KASHYAP and RAO, 1976; etc.) can be expressed in the following form

$$c(t) = \sum_{i=1}^{p} \phi_i c(t-i) - \sum_{i=1}^{q} \theta_i a(t-i) + a(t) \tag{4.1}$$

assuming zero mean for the variable c with variance $s_c^2 = <c^2(t)>$. The a's are a white noise forcing process, which is normally distributed with zero mean and variance $s_a^2 = <a^2(t)>$. The white noise may also be interpreted as the uncorrelated error or residual of one step ahead forecasts.

The observed power spectra (Section 3) and the sample autocorrelation functions (Figure 6) of the first EOF amplitude c_1 suggest that the seasonal time series can be identified as a low order stochastic process because the apparent periodicities are not strong and significant enough compared with red noise. A mixed autoregressive and moving average process can also serve as a possible model because the observed spectral densities and autocorrelations occur in the neighbourhood of AR(1), AR(2) and ARMA (1, 1) processes determined by initial estimates (Figure 6). The pure moving average process MA(q), however, can be excluded from the model building procedure; e.g. MA(1) requires a lag 1 autocorrelation coefficient < 0.5 to obtain real values for the moving average parameter θ_1.

The parameters θ_i, ϕ_i of a sequence autoregressive and mixed autoregressive and moving average models are estimated using the maximum likelihood method. For the summer season the ensemble averaged linear trend has been removed and is added as a deterministic model component. The ARMA (1,1) process appears to be the most adequate fit to the data set; for winter the second order autoregressive model AR(2) is also suitable. Table 1 shows the BIC measures (see Appendix), on which the model selection is based, and the related forecast error estimates (white noise levels), $s_a^2 = <a^2(t)>$, which can be compared with the observed normalized variance $s_c^2 = <c_1^2> = 1$. Fitting higher order ARMA models does not necessarily lead to significantly smaller forecast errors. The ARMA (1,1) models, their power spectra (Figure 6) and time scales

$$\begin{aligned} c(t) &= \phi_1 c(t-1) - \theta_1 a(t-1) + a(t) \\ p(f) &= 2\Delta s_c^2 \frac{1-\phi_1^2}{1+\theta_1^2-2\phi_1\theta_1} \quad \frac{1+\phi_1^2-2\theta_1 \cos 2\pi f\Delta}{1+\phi_1^2-2\phi_1 \cos 2\pi f\Delta} \\ \tau &= \frac{\Delta}{1-\phi_1} \{1-\phi_1 + \frac{(1-\phi_1\theta_1)(\phi_1-\theta_1)}{1-\theta_1^2-2\theta_1\phi_1}\} \sim 4.2 \text{ d} \end{aligned} \tag{4.2}$$

are defined by the following parameter estimates $(\phi_1, \theta_1) = (0.705, -0.344)$ and $(0.745, -0.215)$ for summer and winter fulfilling the conditions of stationarity and invertibility.

Hindcast and independent forecast: Forecasts $\hat{c}_t(l)$ are made by an estimated ARMA model at the origin t for lead time or forecast range l, if c(t–i) and a(t–i) in (4.1) are recursively replaced by $\hat{c}_t(l-i)$ and $\hat{a}(t+l-i)$ starting with nowcasting $\hat{c}_t(0) = c(t)$. Any forecast $\hat{c}_t(l)$ of an ARMA model suffers from the unpredictable noise or error $a(t+1) = c(t+1) - \hat{c}_t(1)$. The expected mean squared forecast error can be derived from (4.1).

$$<a^2(t+l)> = <(c(t+l) - \hat{c}_t(l))^2> = s_a^2 \{1 + \sum_{j=1}^{l-1} \psi_j^2\} \tag{4.3}$$

For extending the forecast range, $l \to \infty$, the forecast error $<a^2(t+l)>$ grows continuously to an upper bound given by the variance of the time series. The ψ_j weights are easily calculated recursively from equation (4.1): $\psi_j = \phi_1 \psi_{j-1} + \ldots + \phi_p \psi_{j-p} - \theta_j$, where $\psi_o = 1$, $\psi_j = 0$ for $j < 0$ and $\theta_j = 0$ for $j > q$.

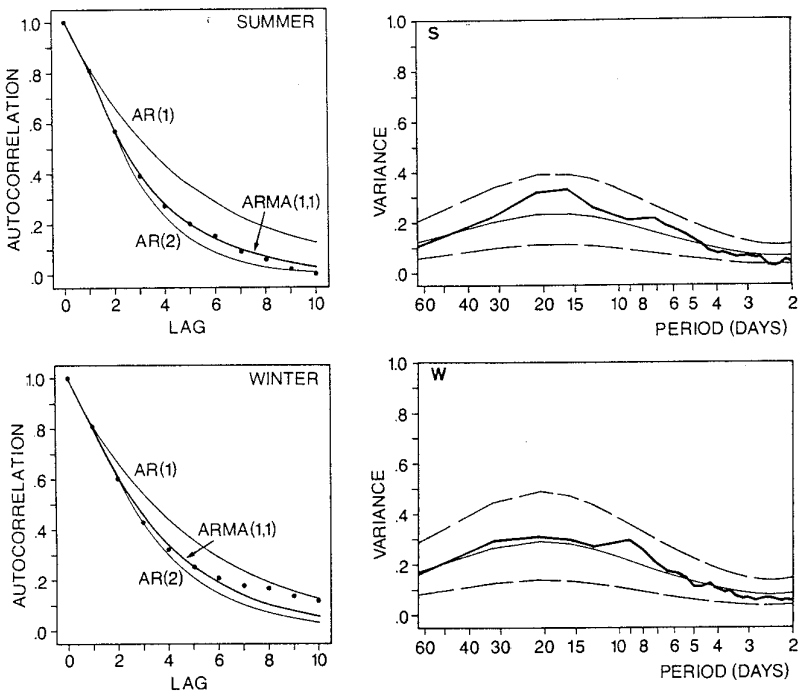

- Figure 6 Left: Autocorrelation of the first eigenvector coefficient c_1 : observed ensemble averages (dots) and various stochastic models fitted to the winter and summer seasons.

  Right: Frequency-multiplied power spectra of the first eigenvector coefficient for summer and winter: observed (full line) and fitted ARMA (1,1) model (fine line) with 95 % significance levels for peaks and gaps (dashed).

- Bild 6 Links: Autokorrelation des ersten Eigenvektor-Koeffizienten c_1 : empirisches Ensemble-Mittel (Punkte) und verschiedene stochastische Modelle, die an die Winter- und Sommer-Jahreszeiten angepaßt sind.

  Rechts: Frequenzgewichtete Power-Spektren des ersten Eigenvektor-Koeffizienten für Sommer und Winter: beobachtet (durchgezogen) und angepaßtes ARMA (1,1) Modell (dünn), sowie 95 % Signifikanz-Niveau (gestrichelt) für Minima und Maxima.

The mean squared error transformed to 500 mbar geopotential height deviations

$$<a^2(t+1)> = <(Z(t+1,\ 500\ \text{mbar}) - Z_1(500\ \text{mbar}) \cdot \hat{c}_t(1))^2>$$

starts with an initial value at the forecast origin t or 1 = 0 (Figure 7), because the first EOF describes the geopotential height at 500 mbar with negligibly small but existing error. With increasing lead time l the stationary and invertible ARMA (1,1) model approaches the ensemble averaged seasonal mean or trend (for summer only) eliminated before model building. Thus, the ARMA forecast $\hat{c}_t(l)$ is attracted by the stationary climate state defined by the first moment of the time series. Consequently, the Gaussian distributed forecast errors grow to an upper limit of zero skill obtained by seasonal mean forecasts. Thus, the ARMA forecast error $<a^2(t+1)>$ and its Gaussian distribution is attracted by the climate state defined by data variance (second moment) and frequency distribution.

The ARMA (1,1) prediction improves the 500 mbar geopotential persistence forecast skill by about 6–7 % in summer but only 3–4 % in winter for one day ahead predictions (Figure 7 and Table 1). A skill of S = 50% appears to be a reasonable lower bound for meteorologically meaningful stochastic prognoses when forecast error and forecast (as derivates from the climate mean state) have equal chance

■ Table 1 The mean squared lead time one forecast error and skill, the information criterion BIC and the portmanteau lack of fit test (Appendix) of various stochastic models predicting the coefficients of the first eigenvector.

■ Tabelle 1 Mittleres Fehlerquadrat und Güte der Eintages-Vorhersage, Informationskriterium BIC und Anpassungstest (Anhang) verschiedener stochastischer Modelle zur Vorhersage des ersten Eigenvektor-Koeffizienten.

	Model	mean squared forecast error (Skill) SU	WI	BIC SU	WI	portmanteau test Q versus χ^2 SU	WI	95 %
hindcast	Persistence	0.32 (67 %)	0.37 (63 %)	−585	−508	124	89	36.4
	AR (1)	0.27 (73 %)	0.34 (66 %)	−671	−559	109	59	36.4
	ARMA (1,1)	0.25 (75 %)	0.325 (67 %)	−710	−574	33	14	35.2
	AR (2)	0.25 (75 %)	0.325 (67 %)	−706	−574	40	14	35.2
	ARMA (2,1)	0.25 (75 %)	0.325 (67 %)	−708	−572	33	13	33.9
	ARMA (1,2)	0.25 (75 %)	0.327 (67 %)	−708	−572	33	13	33.9
	ARMA (2,2)	0.25 (75 %)	0.325 (67 %)	−707	−569	34	18	32.7
forecast	Persistence	0.28 (72 %)	0.70 (42 %)			25	33	
	ARMA (1,1)	0.24 (76 %)	0.57 (53 %)			13	21	

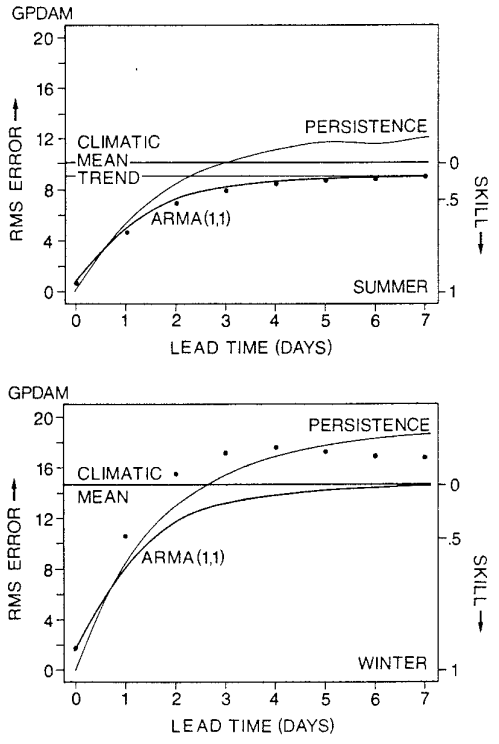

• Figure 7
RMS-error of climatology, persistence and ARMA (1,1) predictions for one to seven days. The independent ARMA (1,1) forecasts of summer 1980 and winter 1980/81 are also included (dots).

• Bild 7
Mittleres Fehlerquadrat der Klimatologie, Persistenz und ARMA (1,1) Vorhersagen für ein bis sieben Tage. Die unabhängigen ARMA (1,1) Prognosen des Sommers 1980 und Winters 1980/81 sind zugefügt (Punkte).

to meet the observations. The ARMA (1,1) model reaches this limit at predictions of about two days ahead. This, of course, lies beyond the persistence forecast quality crossing the zero skill of climatology prediction after the lead time of two days. The ARMA process, however, hardly produces forecast errors of less than zero skill, because the estimated first and second moments hardly change.

The summer 1980 and winter 1980/81 seasons have been omitted from the standard set (used for model fitting) to make independent ARMA (1,1) forecasts (see Figure 7 and Table 1). The first EOF amplitudes c_1 (predictors) are deduced by the standard eigenvectors Z_1 multiplied with the independent daily geopotential heights deviating from the standard mean $<Z>$. The verification measures of the independent summer 1980 forecasts hardly differ from hindcasting the observations (standard set) used for model building. But the winter 1980/81 shows larger discrepancies. They are caused by a shift in the winter 80/81 mean state: Although the first moment hardly changes(i.e. it vanishes), the second moment (variance) differs considerably;it is not unity but $<c_1^2>_{Wi80/81} = 1.2$. This result clearly demonstrates one of the major drawbacks of ARMA prediction applied to meteorology; all seasons deviate more or less from a seasonal mean or standard climate state, particularly if the synoptically active winters are considered. This also explains the relatively low winter hindcast skill of the ARMA models compared with the summer performance. Fitting an independent ARMA (1,1) model to this winter 1980/81 season yields parameters ϕ_1, θ_1 which lie outside the 99 % confidence contour line established in Figure 8 (Appendix). An additional result should be mentioned; the "equivalent barotropic" ARMA (1,1) forecast skill is about 1 to 2 % better than the "barotropic" ARMA (1,1) forecasts, which are directly derived from the 500 mbar geopotential without using the information of the first EOF. Although this result is not surprising it is achieved despite the small initial error made by the EOF transformation.

Forecasting phases of highs and lows: The local pressure or geopotential height trajectory in time defines troughs and ridges passing over a station. It is not so much the local pressure height amplitude or its level, which is of forecast value, but the qualitative behaviour, how a model predicts the lead time of lows and highs. Therefore, observed or predicted lows (or highs) are quantitatively defined by five local pressure height values of consecutive time steps: A low or trough occurs at time t, if its 500 mbar geopotential

$$Z(t) < Z(t \pm l) < Z(t \pm 2) \tag{4.4}$$

achieves a relative minimum between two past and two preceeding neighbours. Thus, a forecast of at least two time steps is required to define a present day (t) geopotential height minimum as a real low, and a forecast of three time steps that tomorrow's minimum is a low, etc. The analogue procedure is applied, if highs or ridges are considered. It is obvious from the definitions of the stochastic processes that an ARMA (1,1) model predicts all extrema to occur within the first forecast time step (l = 0 and l = 1). AR(2) models are able to distribute the predicted extrema over a wider range of lead times, which does not necessarily lead to better forecasts. We evaluate the performance of the ARMA (1,1) and the AR(2) models for the ten winter seasons, when both models produce hindcast skills of comparable magnitude.

A control of the lead time prediction of phases of highs and lows has to be necessary and sufficient:

(i) If lows or highs are observed within lead time l = 0 to l = 1, how many (%) have been predicted?

A total of 91 lows and 87 highs defined by (4.4) is observed in the time series. For daily ARMA (1,1) and AR(2) predictions these reference numbers of lows and highs rise according to the control; i.e. as the lead time l = 0 approaches the observed extremum, a reference low or high may be counted several times, depending on the lead time length considered for the daily forecasts. In this sense ARMA (1,1) and AR(2) models realize 73% (69%) of the observed lows between lead time l = 0 and l = 1, and 73% (73%) between l = 0 and l = 2. They predict 70% (65%) of the highs from l = 0 to l = 1, and 70% (68%) from l = 0 to l = 2 days.

(ii) If lows or highs are predicted within lead time l = 0 to l = 1, how many (%) will be observed? Considering extrema at lead time l = 0 and l = 1, every day ARMA (1,1) and AR (2) forecasts realize a total of 261 (238) lows, 51 % (53 %) of which are observed to occur between lead time l = 0 and l = 1; 62 % (63 %) between l = 0 and l = 2, and 77 % (79 %) between l = 0 and l = 5 days. The ARMA (1,1) and AR(2) models predict 249 (221) highs between l = 0 and l = 1, of which 49% (51%) are observed to occur between lead time l = 0 and l = 1, 57% (60%) from l = 0 to l = 2, and 67% (68%) from l = 0 to l = 5 days.

The results of the control can be summarized as follows. If ARMA or AR models predict a low (high) at short lead times, it will be observed with almost 80% (70%) chance within the following five day period. Additionally, if a low is predicted at these short lead times, a low (but not a high) will be observed, and vice versa. This holds for both controls (i) and (ii).

5 Conclusion and outlook

If the single station geopotential height profiles are confined to the troposphere, the mechanism of stratospheric compensation is excluded and only two eigenvectors (EOF's) are necessary to describe 99% of the vertical and time variability. These two EOF's characterize the barotropic or equivalent barotropic and baroclinic mode of tropospheric dynamics. The associated amplitudes allow a definition of two distinct stochastic time scales related to the dynamic models. The first eigenvectors and their amplitudes can be used as the basis for univariate stochastic prediction of the summer and winter 500 mbar geopotential heights at a single station. A mixed autoregressive and moving average model of first order is selected to perform daily predictions up to a lead time of several days ahead. Higher order models do not lead to a considerable skill improvement, because very high frequency variance (which is implicitly eliminated by the first or equivalent barotropic eigenvector) does not need to be resolved or predicted. The results of the ARMA forecasts may satisfy some practical aspects, because they allow a qualitative lead time prediction of highs and lows. Additionally, they provide a better standard of comparison for NWP models than climatology and persistence, particularly if extended or medium range forecasts are considered. Direct comparison is not yet possible because NWP verifications are generally based on area and not single station rms errors.

Stochastic models may continue to evolve and improve. They would therefore represent increasingly stringent standards of comparison (BAUER and KUTZBACH, 1974). To reduce some of the basic deficiencies of single station stochastic prediction there are some improvements besides an extension in space dimensions: (i) The univariate predictand and predictor can be replaced by a vector variate; such multivariate models may lead to a higher forecast skill; however, the problem of model performance versus model significance arises. (ii) Großwetter related stochastic models may be developed (SPEKAT et al., 1983); e.g. some stochastic models may perform better during situations of high index, others for low index.

Acknowledgement

Thanks are due to Ms. Martina SCHOLZ, Mr. H. HAUG and Ms. C. KIRSCH for typing and drawing and Prof. M. GEB for discussions. Computations and plotting were carried out at the Zentraleinrichtung für Datenverarbeitung (ZEDAT), F. U. Berlin.

Appendix

(i) Stochastic *information criteria* need to be introduced to provide quantitative measures for model order selection demanding parsimony in model building. This ensures that as few θ_i, ϕ_i parameters are estimated as necessary to fit the data adequately.

One objective measure is the Bayesian Information Criterion or BIC (SCHWARZ 1978) which has been applied to ARMA models by KATZ and SKAGGS (1981); accordingly, the orders p and q minimizing

$$BIC(p, q) = n \log < a^2_{p,q}(t) > + (p + q + 1) \log n$$

are selected. The first term on the right hand side is a measure of goodness of fit (mean square error) of the model; the second term is a penalty function for the number of parameters (p + q + 1) required, and n is the number of observations to fit the model. It is not the goal to select the model producing minimum error (as usually done by regression analysis which leads to overfitting) but to penalize error by order to obtain parsimonious models.

(ii) An approximate (1–pr) *confidence region* of the estimated parameters ϕ_1, θ_1 is limited by contour lines

$$s_a^2 \{1 + \frac{\chi^2_{pr}(p + q)}{n}\}$$

measured in terms of model error and defined by the chi-squared distribution $\chi^2_{pr}(K)$ for (p + q) d.o.f. at the probability level pr; (for 1–pr = 99 % and p + q = 2 : χ^2 = 9.21). The relation between the approximate parameter interval of prescribed confidence and the model error is determined by the complete error topography projected into the parameter $\phi_1 - \theta_1$ plane (Figure 8). This is obtained from all ARMA (1,1) processes applied to the data. Even with 99 % confidence the most likely summer and winter parameters (θ_1, ϕ_1) vary so little that they cannot be exchanged for predicting the opposite seasons. The parameter variation decreases, if lower confidence is requested.

(iii) The *portmanteau lack of fit test* (Table 1) selects those models which provide suffiently uncorrelated residuals a(t). The residuals are taken as a whole by $Q = n \sum_{k=1}^{K} < r_a(k) >^2$ with n = 1200 observations to fit the model and tested against a chi-squared distribution χ^2 (K-p-q), with K-p-q degrees of freedom; $r_a(k)$ is the estimated k-lag sample autocorrelation of the white noise residual; for K = 25 lags and a chi-squared distribution at 95% confidence the test is satisfied by the estimated ARMA (1,1) process selected according to the BIC measure.

(iv) A *Gaussian error distribution* or forecast probability density (with zero mean and variance $<a^2(t + 1)>$) can be placed on the forecast (see Figure 9). It diffuses with increasing lead time 1 and

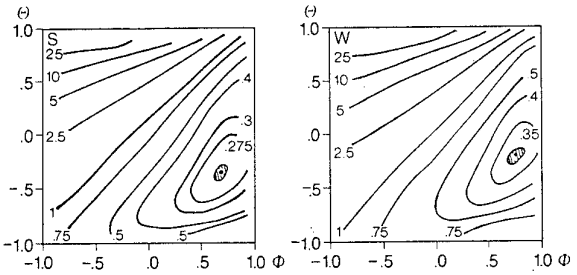

- **Figure 8** Estimated contours of ARMA (1,1) model error and 99% confidence region (shaded) in the (ϕ_1,θ_1) -plane for summer and winter.

- **Bild 8** Geschätzter ARMA (1,1) Modellfehler und 99% Konfidenz-Bereich (schattiert) in der Parameterebene (ϕ_1, θ_1) für Sommer und Winter.

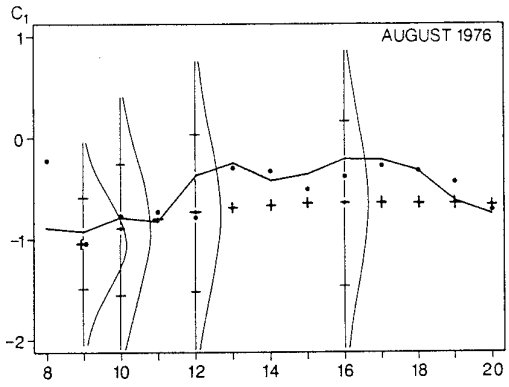

- **Figure 9** Example of a c_1-ARMA (1,1) prediction (8–20 August 1976): Observations (full line), one day ahead predictions (dots), and predictions for lead time $l = 1-12$ (crosses) starting at 8 August. Probability limits (68.3%) and distributions for some lead times ($l = 1,2,4,8$) are included.

- **Bild 9** Beispiel für eine c_1-ARMA (1,1) Vorhersage (8.–20. August 1976): Beobachtungen (durchgezogen), Tagesprognose (Punkte) und Vorhersage für $l = 1$ bis 12 Tage (Kreuze), die am 8. August beginnt. Gaußsche Wahrscheinlichkeits- oder Fehlergrenzen (68.3 %) und Verteilungen für einige Vorhersage-Zeitpunkte ($l = 1,2,4,8$) sind ebenfalls eingetragen.

growing error variance and approaches the (presumed) Gaussian distribution of the data set. Probability limits pr can be attached to each forecast using (4.2). They grow from $s_a \cdot u(pr)$ at lead time $l = 1$ to

$$\hat{c}_t(l) \pm s_a \cdot u(pr) \{1 + \sum_{i=1}^{l-1} \psi_i^2 \}^{1/2}$$

Thus, for the one sigma probability limits, $u(pr = 68.3\ \%) = 1$, there is a pr = 68.3 % chance that observations meet the forecast interval within the positive and negative standard deviation of forecast error about $\hat{c}_t(l)$. With growing lead time, $l \to \infty$, the 68.3 % probability limit of the forecast, $u = 1$, approaches the estimated standard deviation of the data set, $s_c = <c^2>^{1/2}$. Other probability limits are $u(pr = 50\%) = 0.674$, $u(pr = 95\ \%) = 1.96$ etc. An August 1976 period (discussed in Section 2) is selected to present a direct application of a stochastic or ARMA (1,1) prediction up to a lead time of 12 days. This hindcast example includes the estimated probability distribution and confidence limit changing with increasing lead time (Figure 9).

List of Symbols

$Z(t, p)$, $Z_{1,2,3}(p)$	geopotential height; first, second and third eigenvector of geopotential height
p, t, f	pressure, time, frequency $0 \leqslant f \leqslant 1/2\Delta$
$c(t)$, $c_{1,2}(t)$, λ^2	time-dependent coefficient or amplitude of eigenvector Z_1 or Z_2, eigenvalue
s_c^2, $<\sigma^2>$	time variance of c_1, space-time variance
ϕ, θ, p, q	parameters and order of ARMA model
AR, MA, ARMA; p(f)	autoregressive, moving average and mixed stochastic model; related power spectrum
$a(t)$; $s_a^2 = <a^2(t)>$	error, residual or white noise; its estimated variance
$\tau = \Delta \sum_{k=0}^{\infty} <c(t)c(t-k)>/<c^2(t)>$	integral-, macro- or relaxation time scale
Δ	time step 1 day
$<>$; [ ]	seasonal time or ensemble average; area average (section 2 only)
$\hat{c}_t(l)$	forecast estimate of c_1 starting at time t for lead time l
S, rms	skill, root mean square
χ^2, u(pr)	chi-squared distribution, deviate exceeded by proportion pr of the unit Gaussian distribution

References

BAUER, G. K. and J. E. KUTZBACH, 1974: Evaluation standards for dynamical prediction models. J. Appl. Meteor. 13, 505–506.

Berliner Wetterkarte, 1976: Beilage 99/76 (KEU VIII/76) and Beilage 100/76 (KNH VIII/76).

BOX, G. E. P. and G. M. JENKINS, 1976: Time series analysis. Holden-Day, 575 pp.

BÖTTGER, H. and K. FRAEDRICH, 1980: Disturbances in the wavenumber-frequency domain observed along 50° N. Beitr. Phys. Atmosph. 53, 90–105.

FRAEDRICH, K. and K. MÜLLER, 1983: On single station forecasting: sunshine and rainfall Markov chains. Beitr. Phys. Atmosph. 56, 108–134.

GAVRILIN, B. L., 1965: On the description of vertical structure of synoptical processes. Jzv. Atmos. Oceanic Phys. 1, 4–8.

GREEN, J. S. A., 1977: The weather during July 1976: Some dynamical considerations of the drought. Weather 32, 120–128.

HAYASHI, Y. and D. G. GOLDER, 1977: Space-time spectral analysis of mid-latitude disturbances appearing in a GFDL general circulation model. J. Atmos. Sci. 34, 237–262.

HOLMSTRÖM, I., 1963: On a method for parameteric representation of the state of the atmosphere. Tellus 15, 127–149.

JENKINS, G. M. and D. G. WATTS, 1968: Spectral analysis and its applications. Holden-Day Inc. San Francisco, 525 pp.

KASAHARA, A., 1976: Normal models of ultralong waves in the atmosphere. Mon. Wea. Rev. 104, 669–690.

KASHYAP, R. L. and R. A. RAO, 1976: Dynamic stochastic models from empirical data. Acad. Press, 334 pp.

KATZ, R. W. and R. H. SKAGGS, 1981: On the use of autoregressive-moving average processes to model meteorological time series. Mon. Wea. Rev. 109, 479–484.

SCHWARZ, G., 1978: Estimating the dimension of a model. Ann. Statist. 6, 461–464.

SPEKAT, A., B. HELLER-SCHULZE and M. LUTZ, 1983: Über Großwetter und Markov-Ketten. Met. Rdsch., in press.